Designing orbital and charge ordering multiferroics by superlattice strategy and strain engineering

Yajun Zhang [1,2,*] Peng Han [3] M. P. K. Sahoo,[4] Xu He,[5] Jie Wang,[3] and Philippe Ghosez [5]

[1]*Key Laboratory of Mechanics on Disaster and Environment in Western China, Ministry of Education of China,*
Lanzhou University, Lanzhou, Gansu 730000, China

[2]*Department of Mechanics and Engineering Sciences, College of Civil Engineering and Mechanics,*
Lanzhou University, Lanzhou, Gansu 730000, China

[3]*Department of Engineering Mechanics and Key Laboratory of Soft Machines and Smart Devices of Zhejiang Province,*
Zhejiang University, 38 Zheda Road, Hangzhou 310027, China

[4]*Department of Physics, Veer Surendra Sai University of Technology, Burla, Odisha, 768017, India*

[5]*Theoretical Materials Physics, Q-MAT, CESAM, Université de Liège, B-4000 Liège, Belgium*

Orbital ordering (OO) or charge ordering (CO) in e_g^1 compounds like RMnO$_3$ (R = rare-earth element), RNiO$_3$, and CaFeO$_3$ makes them attractive functional materials. Despite belonging to the e_g^1 family, SrFeO$_3$ is metallic and free from OO and CO, which may limit its technological potential. Here, through first-principles calculations, we propose a rational design of OO and CO insulating SrFeO$_3$ by superlattice strategy and strain engineering. With a systematical investigation of the interplay among Jahn-Teller distortion related to OO, breathing distortion associated with CO, strain, octahedral rotations, and cation ordering, we reveal that cation ordering in SrFeO$_3$/ABO$_3$ superlattices not only is capable to stabilize Jahn-Teller and breathing distortions, but is also indispensable in triggering metal-insulator transition by the collaboration with Jahn-Teller or breathing distortion, leading to ferromagnetic insulating SrFeO$_3$. Owing to the different sensitivity of Jahn-Teller and breathing distortions to strain, purposeful design of OO or CO phase and even as multiferroics coexisting ferro-electric and ferromagnetic orders can be realized by tuning the relative stability of CO and OO phases by strain engineering. The coupled charge, orbital, spin, and ferroelectricity degrees of freedom make SrFeO$_3$/ABO$_3$ superlattices appealing for desired applications.

I. INTRODUCTION

Orbital ordering (OO) characterized by Jahn-Teller distortion (JTD) and charge ordering (CO) characterized by breathing distortion (B_{oc}) in e_g^1 (with only one electron/hole on the e_g orbital) perovskites have attracted considerable attention since they often produce fascinating phenomena such as high-T_c superconductivity [1–3], colossal magnetoresistance (CMR) [4,5], and metal-insulator transition (MIT) [6–8]. It is well known that RMnO$_3$ (R = rare-earth element) remove the orbital degeneracy by forming the OO phase [9–12], while RNiO$_3$ (RNO) [13–16] and CaFeO$_3$ (CFO) [17–19] undergo a charge disproportionation showing CO state. Regarding SrFeO$_3$ (SFO), despite the same e_g^1 electronic configuration, it keeps the same cubic metallic phase down to 4.2 K without CO or OO transition [20]. Stemming from the extensive CO and OO based applications, it is important to gain a better understanding of the microscopic details of SFO and pursue external perturbations to trigger CO or OO transition in order to extend its functionality.

In perovskites, tolerance factor t is an important factor that determines the rotations of oxygen octahedra. When $t < 1$, perovskites distort from the cubic structure and the smaller the t value, the larger the amplitude of octahedral rotations. The structural, electronic, and magnetic properties of perovskites are strongly sensitive to rotations due to phonon-phonon coupling, electron-phonon coupling, and spin-phonon coupling. Lee *et al.* proposed that the phonon-phonon coupling between rotations and JTD is critical in stabilizing the OO phase in ferromagnetic (FM) LaMnO$_3$ [21], which is the magnetic ground state (GS) of LaMnO$_3$ thin film grown on SrTiO$_3$ (STO) substrate [22]. Just recently, we highlighted that B_{oc} and CO in CFO are triggered by the cooperative biquadratic coupling with rotations [23], which is in line with the origin of CO in RNO found by Mercy *et al.* [24]. Strain is another factor that controls the electronic and structural properties of e_g^1 perovskites; recent works show that tensile strain can switch RNO and CFO from CO to OO phase [23,25,26]. Cherair *et al.* also show that epitaxial strain can induce JTD and OO phase in BaFeO$_3$ [27]. These illuminating findings thereby offer the prospect of inducing CO or OO by rotations or strain engineering in SFO.

The superlattice strategy provides a promising platform to achieve rotations and strain conditions. On the one hand, due to the propagation of rotations at the interface, rotations could transfer from one layer to another layer [28–31]. For example, the rotations from STO propagating into the SFO layer in (STO)$_n$/(SFO)$_1$ superlattices is predicated by Rondinelli *et al.*; they also demonstrate that quantum confinement effect produced by the superlattice strategy enhances the electron-lattice instabilities and orbital degeneracy lifting [30,31]. On the other hand, depending on the composition of superlattices,

*zhangyajun@lzu.edu.cn

different strain conditions can be realized by lattice mismatch and epitaxial growth. Moreover, the superlattices provide an extra degree of freedom to create multiferroics based on the hybrid improper ferroelectricity mechanism [32,33]. Motivated by the above benefits of superlattices and the dramatic advance in modern growth techniques [7,34], it is particularly interesting to fully understand the couplings and competitions among rotations, strain, charge, orbital, and polar mode in SFO based superlattices. More importantly, it will greatly benefit device applications if guidance on purposefully inducing OO and CO multiferroics could be formulated.

In this work, we propose a material design strategy to realize OO and CO multiferroics in SFO based superlattices. First, we give a deep understanding of how strain and rotations control the stability of JTD and B_{oc} in bulk SFO. It is found that tensile strain softens JTD and compressive strain stiffens it. In contrast, the stability of B_{oc} is less sensitive to both tensile and compressive strain. In terms of rotations, similar to our previous finding that rotations could stabilize B_{oc}, we demonstrate that rotations also notably soften JTD. The superlattice strategy is then harnessed to tune the strain and rotations of SFO. We found that strain plays a similar role in the superlattices as in SFO thin film, while rotations become ineffective and hardly affect the stabilization of JTD and B_{oc}. Additionally, we unveil that the cation ordering induced quantum confinement effect is critical in the softening of two distortions. Based on our knowledge, we demonstrate that superlattices which support tetragonal tensile strain and quantum confinement effect like SFO/CaTiO$_3$ (CTO), make the FM OO phase the GS. To achieve a stable FM CO phase, smaller tetragonal strain and strong quantum confinement are essential, as in SFO/YAlO$_3$ (YAO) superlattices grown on YAO substrate. Further study reveals that it is possible to achieve polar distortion in SFO/ABO$_3$ superlattices by selecting the ABO$_3$ layer with a different A-site atom and $a^- a^- c^+$ rotation patterns to make FM SFO/ABO$_3$ multiferroics.

II. METHODS

First-principles calculations were carried out using density functional theory (DFT) within the generalized gradient approximation (GGA) using the PBEsol functional [35] as implemented in the Vienna *ab initio* simulation package (VASP) [36,37]. To account for the strong correlation effects, on-site Coulomb repulsion $U = 7.2$ and exchange interaction $J = 2$ were applied for the Fe $3d$ states [38]. We used a relatively high plane-wave cutoff energy of 600 eV and $8 \times 8 \times 6$ Monkhorst-Pack k-point mesh [39] for a $\sqrt{2} \times \sqrt{2} \times 2$ supercell with different magnetic orderings. During the structural optimizations, the lattice parameters and internal coordinates of atoms were fully relaxed until the Hellmann-Feynman forces on each atom were less than 10^{-4} eV/Å. The ferroelectric (FE) polarization was calculated by the Berry-phase methods [40] and the mode amplitudes were identified by the ISODISTORT software [41,42]. The *ab initio* molecular dynamics (AIMD) simulations in NVT ensemble were carried out at 1000 K by using the Andersen thermostat. A $3 \times 3 \times 3$ supercell with Γ-point sampling was used and the total simulations last for 24 ps with a time step of 2 fs.

III. RESULTS AND DISCUSSION

A. Strain and rotation tuned Jahn-Teller and breathing distortions

Before studying the properties of SFO based superlattices, we examine systematically the bulk properties and how epitaxial strain and rotation would affect the stability of JTD and B_{oc}. To determine the minimum-energy magnetic configuration, SFO with cubic symmetry is fully relaxed in four collinear spin configurations, namely FM state, A-type, C-type, and G-type antiferromagnetic (AFM) states. We confirm that FM phase is the most preferred state consistent with previous theoretical results [43] and the lattice constant of 3.84 Å is in close agreement with the experimental value of 3.85 Å [20]. The phonon spectrum analysis in our previous work [23] indicates that the cubic phase is the GS structure and the dynamical stability of the structure at 1000 K is ensured by the AIMD simulations (see Fig. S1 in Supplemental Material (SM) [44]).

Now we discuss the effect of epitaxial strain induced by a square lattice substrate on the phase transition of SFO; the amplitude of strain ε is defined as $\varepsilon = (a - a_0)/a_0$, in which a_0 is the lattice constant of the GS structure and a is the in-plane lattice constant of the substrate. During the structural relaxation, the in-plane lattice constant is fixed, and the out-of-plane lattice constant and all the atomic positions are fully relaxed. To identify the GS structure under different strains, we perform relaxation of various distorted structures by condensing individual or coupled phonon modes. The modes considered include (i) JTD M_{JT} (irreps M_3^+) as displayed in Fig. 1(a); (ii) B_{oc} (irreps R_2^-) as shown in Fig. 1(b); (iii) in-phase rotation M_z [Fig. 1(c)] along the [001] axis (irreps M_2^+); (iv) out-of-phase tilt R_{xy} [Fig. 1(d)] around the [110] axis (irreps R_5^-); and (v) out-of-phase rotation R_z along the [001] axis (irreps R_5^-). Epitaxial biaxial strain induced volumetric strain Q_1^Γ and tetragonal strain Q_3^Γ modes are plotted in Figs. 1(e) and 1(f), respectively.

The energy difference between the lowest energy phases and the high-symmetry cubic (0% strain state) or $P4/mmm$ phase (strained state) is plotted in Fig. 2(a). As can be seen, the high-symmetry cubic or $P4/mmm$ phase remains the GS and there is no unstable mode when strain ranges from -1% to 3%. When tensile strain is further increased, it is found that the energy of the $P4/mbm$ phase characterized by JTD is lower than that of the $P4/mmm$ phase and the energy difference increases as strain increases, indicating JTD can be induced by tensile strain. In terms of compressive strain, the out-of-phase rotation R_z is stabilized and reducing the symmetry to $I4/mcm$ phase when compressive strain is larger than 1%. In contrast, the B_{oc} is unfavored over the whole strain range.

In order to gain a deeper insight into the origin of strain induced JTD, we first explore the dynamical stability of JTD under different strain states. Figure 2(b) shows the potential energy surface (PES) as a function of JTD amplitude (Q_{JT}). For each strain state, we fix the lattice constant to be the same as that of the lowest energy structure under strain, as shown in Fig. 2(a). It should be noted that the amplitude of phonon motion can be described by Å (normalized to the parent cell) as used in the ISODISTORT software [41,42] or Å/$\sqrt{\text{amu}}$ as used in the PHONOPY code [45] and Ref. [46] (amu is atomic
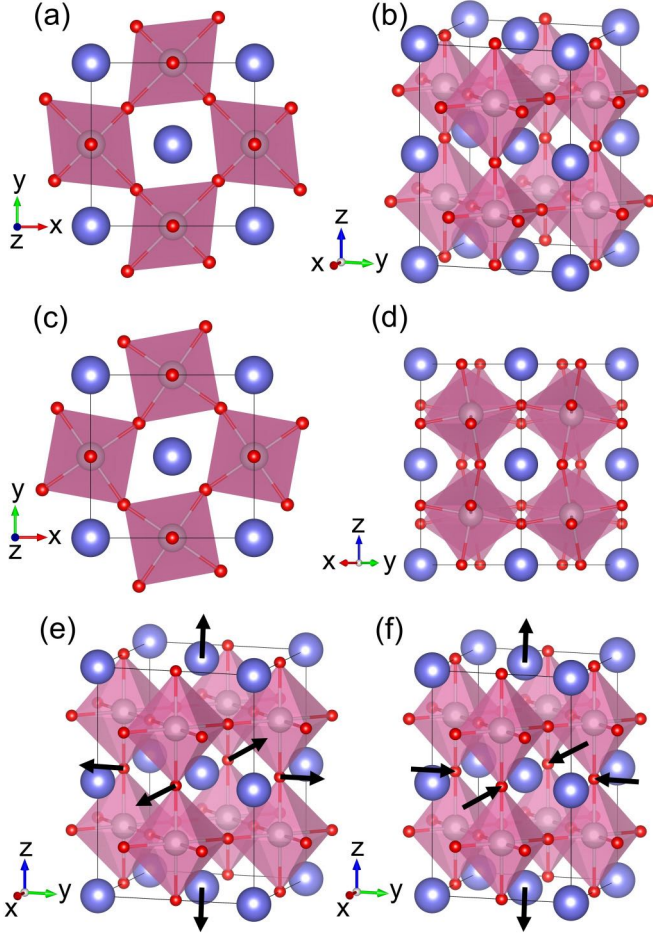
FIG. 1. Schematics of (a) Jahn-Teller distortion, (b) breathing distortion, (c) in-phase rotation, (d) out-of-phase tilt, (e) volumetric strain, and (f) tetragonal strain mode. JTD results from the alternative elongation and contraction of two in-plane bonds in the same oxygen octahedra, and is accompanied by the OO transition, and the B_{oc} mode can be described by the alternative elongation and contraction of the B-O bonds along three directions in two neighboring BO_6 octahedra. The inwards arrow and outwards arrow denote the decrease and increase of lattice constant, respectively.

mass units). For the investigated coupling between different distortions, the strain modes are also considered. To clearly show the coupling between strain mode and phonon distortion by analyzing the coupling coefficients, we would use the same unit of Å for the strain and phonon modes as quantified by the ISODISTORT software.

It is clear that compressive strain disfavors JTD and tensile strain gradually softens JTD, and it becomes unstable at 4% tensile strain. We next explore in detail how strain and JTD are coupled by performing a symmetry-adapted mode analysis. With the help of the ISODISTORT program [41,42], we propose that epitaxial tensile strain can be decomposed into volumetric strain Q_1^Γ and tetragonal strain Q_3^Γ modes as described in Figs. 1(e) and 1(f), respectively. Here, we define the volumetric strain that leads to a volumetric increase (decrease) as positive (negative) value. Similarly, tetragonal strain for which in-plane lattice constant decreases (increases) and out-of-plane lattice constant increases (decreases) is de-

TABLE I. The coefficients of the PESs of JTD and breathing distortion, and the coefficients of different phonon-strain coupling terms in units of meV/$Å^n$, where n is the order of the energy term.

Q_{JT}	α_{JT}	β_{JT}	Q_B	α_B	β_B
	1955	16 664		2084	75 705
Q_{JT}-Q_1^Γ	γ_{1JT}	δ_{1JT}	Q_B-Q_1^Γ	γ_{1B}	δ_{1B}
	−41 968	91 466		18 886	171 568
Q_{JT}-Q_3^Γ	γ_{3JT}	δ_{3JT}	Q_B-Q_3^Γ	γ_{3B}	δ_{3B}
	29 614	33 374		−303	181 228

fined as a positive (negative) value. Using group theory, the energy related to JTD can be derived as

$$E_{JT} = \alpha_{JT}(Q_{JT})^2 + \beta_{JT}(Q_{JT})^4 + \gamma_{1JT}Q_1^\Gamma(Q_{JT})^2$$
$$+ \delta_{1JT}(Q_1^\Gamma)^2(Q_{JT})^2 + \gamma_{3JT}Q_3^\Gamma(Q_{JT})^2$$
$$+ \delta_{3JT}(Q_3^\Gamma)^2(Q_{JT})^2 \tag{1}$$

We note that the breathing distortion has the same coupling terms with volumetric strain and tetragonal strain. The individual energetic contributions of Q_1^Γ and Q_3^Γ modes (the same amplitude as their GS under strain) in stabilizing the JTD and B_{oc} are plotted in Figs. 2(c)–2(g). The coefficients of different phonon-strain coupling terms are listed in Table I and the PESs obtained from first-principles calculations and the fitting results are compared in Figs. S2– S5 in SM [44]. The results in Figs. 2(c) and 2(d), as well as Table I indicate that positive Q_1^Γ and negative Q_3^Γ strain modes produced by tensile strain both give rise to the energy lowering of JTD. Despite each of them not being strong enough to destabilize the JTD, their combined effects make it appear at 4% tensile strain. As a comparison, we find that B_{oc} is weakly coupled with strain modes compared with JTD as reflected in Table I, and the PESs are only slightly affected by epitaxial strain, and Q_1^Γ and Q_3^Γ strain modes as shown in Figs. 2(e)–2(g).

Rotation motions including in-phase rotation M_z (Q_M) and out-of-phase tilt R_{xy} (Q_R) may also be key factors that control JTD. As revealed in our previous work, B_{oc} is progressively stabilized by artificially fixing rotations in SFO by the $\lambda_{MB}Q_M^2Q_B^2 + \lambda_{RB}Q_R^2Q_B^2$ coupling [23]. We also highlight that rotation can help stabilize JTD in CFO. To examine whether the coupling between rotation and JTD still applies for SFO, we plot in Fig. 2(h) the energy change associated with JTD by fixing different percentages of rotations that correspond to the GS values in CFO. We find that even though 100% rotations are insufficient to stabilize JTD, the energy cost of JTD is significantly decreased. The results also indicate that larger rotations beyond CFO are possible to stabilize JTD. The coupling between rotations and JTD can be expressed as $\lambda_{MJT}Q_M^2Q_{JT}^2 + \lambda_{RJT}Q_R^2Q_{JT}^2 + \lambda_{MRJT}Q_MQ_R^2Q_{JT}$.

B. Engineering metal-insulator transition by orbital ordering

Despite being stabilized under tensile strain in SFO, JTD is still insufficient to open the band gap, and the system remains metallic even under 4% tensile strain. To trigger the insulating phase in SFO, we suggest that two key factors should be
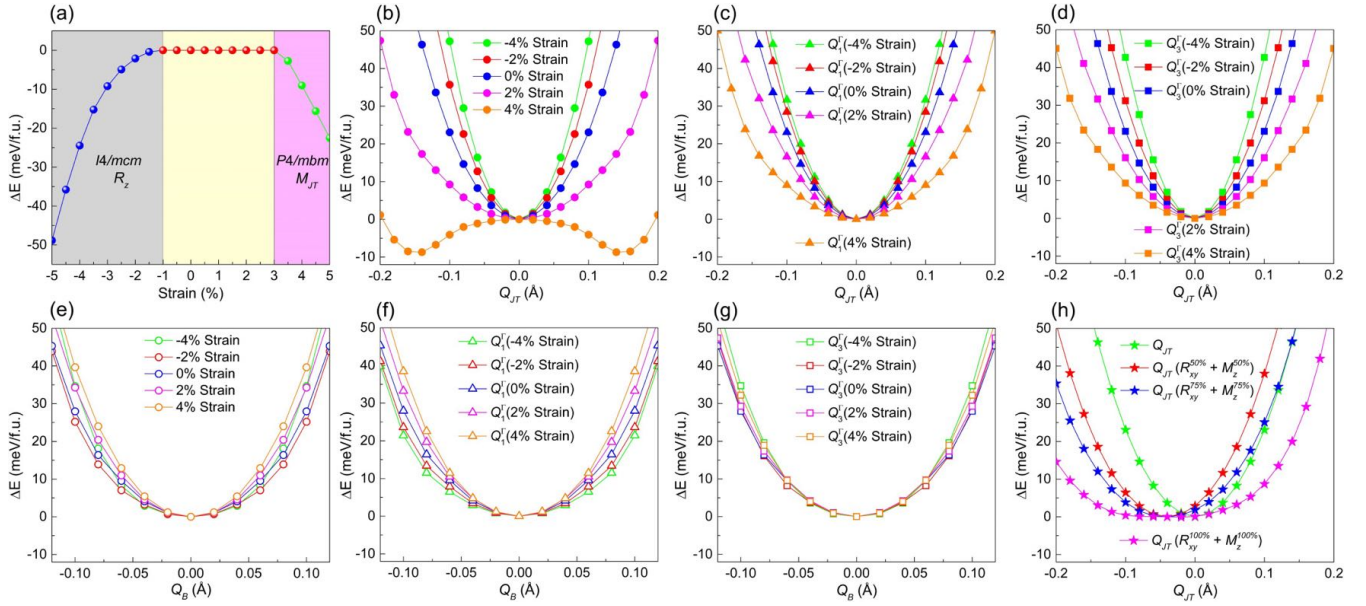
FIG. 2. (a) Phase diagram of SFO under epitaxial strain. (b)–(d) PESs with respect to the JTD amplitude (Q_{JT}) at fixed (b) lattice constant, (c) volumetric strain (Q_1^Γ), and (d) tetragonal strain (Q_3^Γ) of each strained state. (e)–(g) The corresponding PESs with respect to the B_{oc} amplitude (Q_B) of each strained state. (h) PES with respect to the JTD amplitude at fixed rotations (M_z) and tilts (R_{xy}) of 50%, 75%, and 100% of the amplitudes (0.41 and 0.57 Å) of FM CFO.

addressed: (i) mode coupling between JTD and strain or rotations, which is indispensable to induce JTD; (ii) the breaking of long-range FM interactions along the z direction. The second factor originates from the metallic nature of the FM state and the insulating nature of the A-AFM state in OO LaMnO$_3$ [21] and CFO under tensile strain [23].

Superlattices like SFO/CTO present a promising paradigm to induce JTD through strain, rotations, and quantum confinement effect. The long-range FM interactions along the z direction are broken by cation ordering and form the ↑ 0 ↑ 0 arrangement. Fully optimized SFO/CTO superlattices are found to be the monoclinic Pc phase containing notable in-phase rotation, out-of-phase tilt, JTD, and polar distortions. Comparison of the energy of FM and AFM states confirms the FM state is the lowest energy magnetic order. The projected density of states (PDOS) shown in Fig. 3(a) indicates that the degenerate electronic state are broken and there is a higher occupation of $d_{3x^2-r^2}$ band than the $d_{y^2-z^2}$ band due to the alternating long and short Fe-O distance, an indication of OO state. To clarify the stability of JTD, we first analyze the PESs of rotation, tilt, and JTD with respect to the reference $P4mm$ phase. As shown in Fig. 3(b), all three distortions, even JTD, exhibit double-well potential energy, indicating their intrinsic nature and spontaneous appearance. To provide further support for the design of OO SFO in experiments, it is interesting to ascertain the precise origin of JTD in SFO/CTO superlattices. We now examine the role of quantum confinement effect induced by cation ordering. To eliminate the strain effect, we simply replace one layer SFO by CTO in full relaxed $\sqrt{2} \times \sqrt{2} \times 2$ SFO supercells, then the change in total energy as a function of JTD is plotted as shown in Fig. 3(c). Consistent with previous work on (STO)$_n$/(SFO)$_1$ superlattices [30,31], the energy curve exhibits a characteristic double-well potential, which indicates that JTD and the accompanied OO

state could emerge as a consequence of the cation ordering. However, we find that the energy lowering of JTD driven by the confinement effect is much smaller than that with respect to the $P4mm$ reference [green curve Fig. 3(c)]. A more detailed structural analysis indicates the presence of negative tetragonal strain in the SFO layer that further strengthens the OO GS by $\gamma_{3JT} Q_3^\Gamma (Q_{JT})^2 + \delta_{3JT} (Q_3^\Gamma)^2 (Q_{JT})^2$ coupling. It is noteworthy that, although the misfit strain between CTO and SFO is negligible when comparing their pseudocubic lattice parameters, the Ti ion with larger radius suppresses the out-of-plane O-Fe-O bond length, resulting in a c/a ratio of 0.965 in the SFO layer which plays a role similar to tetragonal strain produced by tensile strain in the SFO thin film. To further evaluate the contribution of rotations, energy evolution of JTD with fixed in-phase rotation and out-of-phase tilt is plotted in Fig. 3(c); it can be found that the energy lowering and the mode amplitude with the minimum energy only slightly increase. Therefore, we can draw the conclusion that cation ordering induces the OO state, and tetragonal strain in the superlattices further stabilizes it.

Besides the OO character, we find that the superlattices are insulating as expected. To investigate the role of each factor in opening the band gap, we analyzed the band structure of the superlattices under various conditions as shown in Fig. 4. The band structure of the strain-free metallic cubic phase is illustrated in Fig. 4(a) for comparison. With the presence of 4% tensile strain and JTD shown in Fig. 4(b), we find that JTD has a significant effect on the electronic structure, and band structure along partly paths of the Brillouin zone is opened, while the band structure especially along the Γ-Z path remains closed and the whole system is metallic. Interestingly, although remaining metallic along most paths, the B-site Fe/Ti cation ordering happens to open the gap along Γ-Z path, as shown in Fig. 4(c). As expected, through
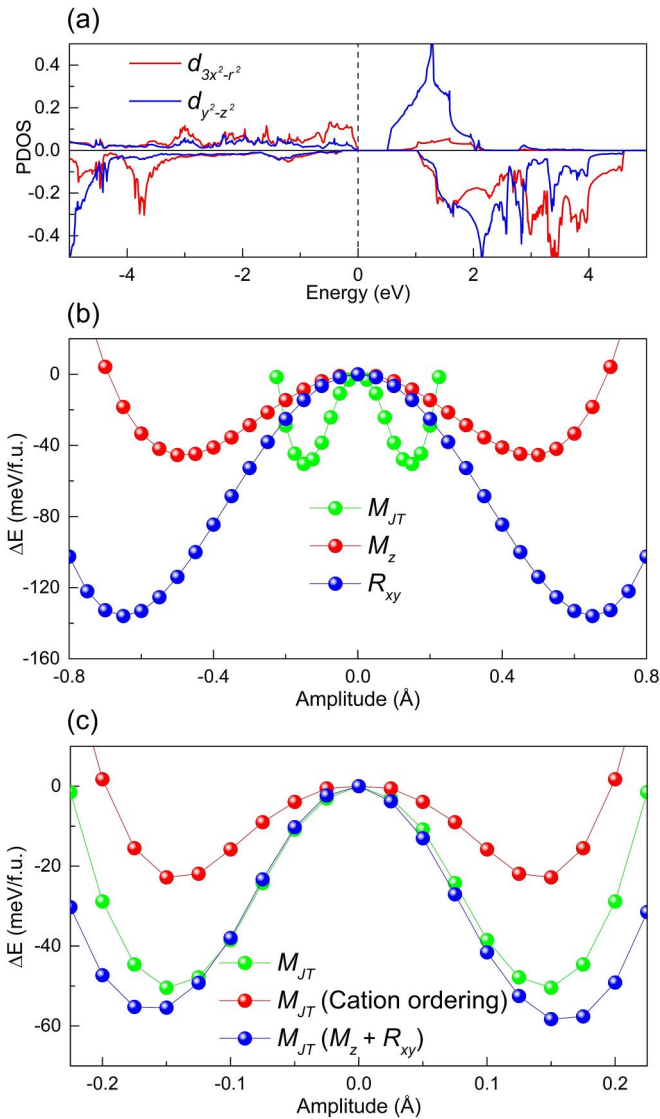
FIG. 3. (a) PDOS of OO SFO/CTO superlattice. (b) PESs with respect to the amplitude of JTD, in-phase rotation (M_z), and out-of-phase tilt (R_{xy}) in SFO/CTO superlattices. (c) PESs with respect to the JTD amplitude at fixed cation ordering (CTO layer) and rotation and tilt with amplitudes in the GS structure.
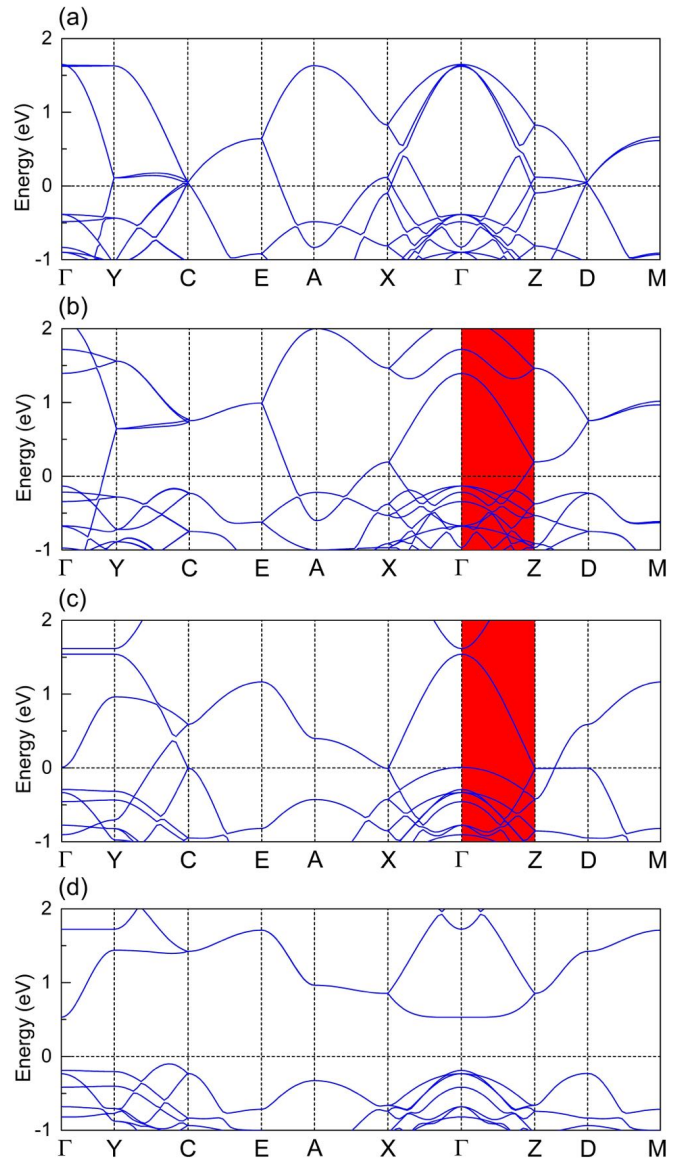

FIG. 4. The band structure of (a) strain-free cubic SFO, (b) cubic SFO with JTD at 4% tensile strain, (c) SFO/CTO superlattice without distortions, and (d) SFO/CTO ground state superlattice.

the combination of this cation ordering with JTD, metallic SFO/CTO becomes insulating as reflected in Fig. 4(d). We may, therefore conclude that both JTD and B-site cation ordering are indispensable to induce the insulating phase.

C. Engineering metal-insulator transition by charge ordering

Besides OO, CO is also an effective way to form an insulating phase, as observed in RNO [14] and CFO [17,18]. In our previous work, we proposed that if rotations could be stabilized in SFO it is possible to stabilize B_{oc} and realize an insulating state [23]. To realize practically this idea, we select YAO as a component of the SFO/ABO$_3$ superlattices, because YAO has strong rotations and less mismatch strain with SFO to avoid the tensile epitaxial strain induced OO state.

With the condensation of rotations and B_{oc}/JTD, we fully relax the structures. It is interesting to find that both CO and OO insulating phases could be stabilized with the OO phase as the lowest-energy structure. The FM ordering is found to be lower in energy in both CO and OO SFO/YAO superlattices. It remains intriguing why SFO prefers to exhibit OO rather than CO phase when combined with YAO containing smaller in-plane lattice mismatch. To reveal and understand the physical origin of the OO state, we first check the structural character of the superlattices. We find that the O-Al-O bond length along the z direction is 3.86 Å larger than the value of 3.75 Å for O-Fe-O. The average of two in-plane O-Fe-O bond lengths is 3.88 Å; this indicates that there exists negative tetragonal strain in the SFO layer, which tends to stabilize the JTD and OO phase.
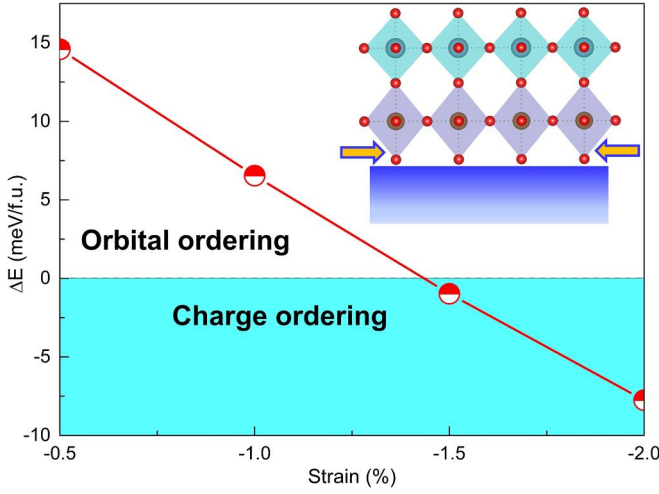
FIG. 5. Phase diagram of the OO-CO transition in SFO/YAO superlattices described by the energy difference between two phases.
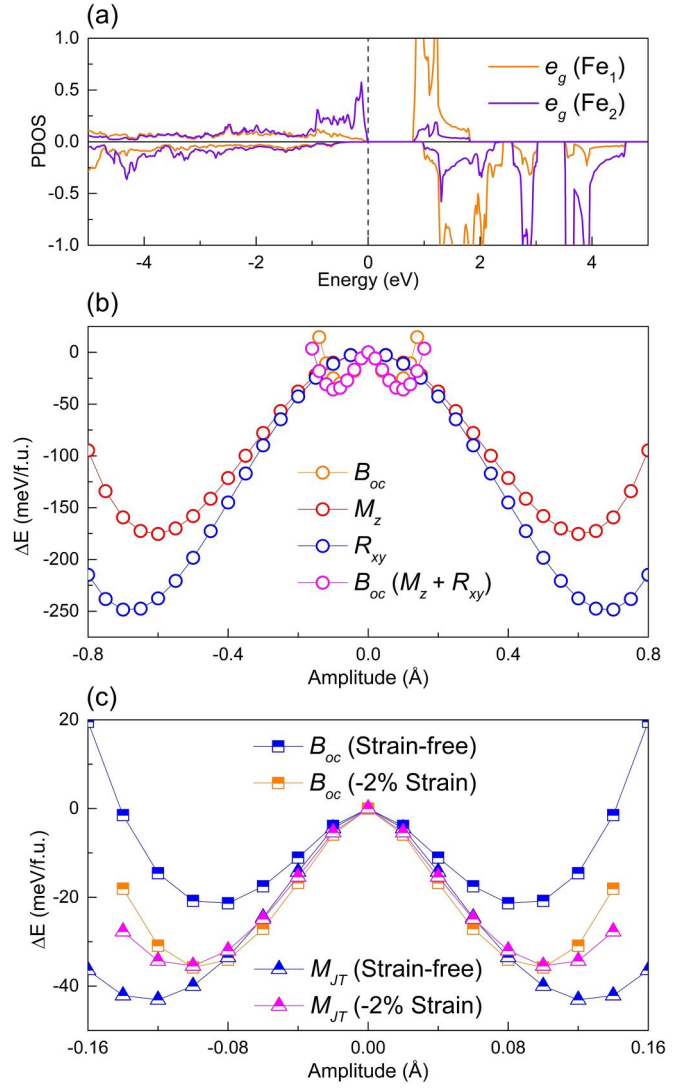

FIG. 6. (a) PDOS of CO SFO/YAO superlattice under 2% compressive strain. (b) PESs with respect to the amplitude of B_{oc} (with and without fixed rotation and tilt), in-phase rotation (M_z), and out-of-phase tilt (R_{xy}) in the SFO/YAO superlattices under 2% compressive strain. (c) PESs with respect to the JTD/B_{oc} amplitude for SFO/YAO superlattices without strain and under 2% compressive strain.

Despite OO state being the energetically favorable phase, we find that the CO phase is just higher in energy by 26 meV/Fe. We wonder whether it is possible to tune the relative stability of OO and CO phases and engineer CO phase as the GS, which is not only physically interesting but also promising for applications.

With the knowledge in the above sections that the energy lowering of JTD is highly sensitive to strain, while the energy of B_{oc} is less sensitive to strain, we anticipate that decreasing the negative tetragonal strain by epitaxial compressive strain produced by the substrate might favor the CO phase. To realize practically this idea, we investigated how epitaxial compressive strain from 0.5% to 2% tunes the total energy of OO and CO phases, which is displayed in Fig. 5. The same relaxing strategy is employed as for the SFO thin films to identify the GS structure under different strains. The results validate our hypothesis: when strain is beyond 1.5%, the GS of the superlattices changes from the OO phase to the CO phase. Figure 6(a) displays the electronic structure of two e_g states at neighboring FeO$_6$ cages; the spin polarization of the Fe$_2$ atom with a larger Fe-O bond length is much stronger than that of the Fe$_1$ atom with smaller Fe-O bond length, a clear indication of CO state. Thus, epitaxial strain can be harnessed to tune the physical behavior of SFO/YAO superlattices, which provides new perspective for designing CO functional materials.

In order to better understand the strain induced phase transition, we first discuss the origin of B_{oc} in SFO/YAO superlattices with 2% compressive strain. The evolution of the total energy as a function of B_{oc} amplitude is shown in Fig. 6(b); a notable energy lowing is observed with the appearance of B_{oc}, which can also be attributed to the confinement effect. We also confirm that rotation and tilt propagate from the YAO layer to the SFO layer and make significant contributions to the GS as plotted in Fig. 6(b). Then, we analyze whether rotation and tilt are responsible for stabilizing the CO phase as we proposed in bulk SFO [23]. One can notice that, in Fig. 6(b), further condensing of rotation and tilt just slightly increases the energy lowering of B_{oc} and the distortion amplitude with the lowest energy.

Now we pay our attention to the explanation of strain induced OO-CO transition; Fig. 6(c) shows the change of energy as a function of B_{oc} and JTD for strain-free and 2% compressive strain states. Without strain, it is clear that the energy lowering related to JTD is larger than that of B_{oc}. With 2% compressive strain, we observe that the energy lowering associated with JTD is substantially decreased and becomes smaller than that of B_{oc} which slightly increases. As a consequence, the CO state becomes the most energetically favored phase. Then, we evaluate the actual contribution of cation ordering and breathing distortion toward affecting the band structure. Taking cubic SFO as a reference, the band structure with cation ordering, B_{oc}, and both factors are plotted in Fig. 7. Similarly to the effect of JTD and cation ordering, we find that
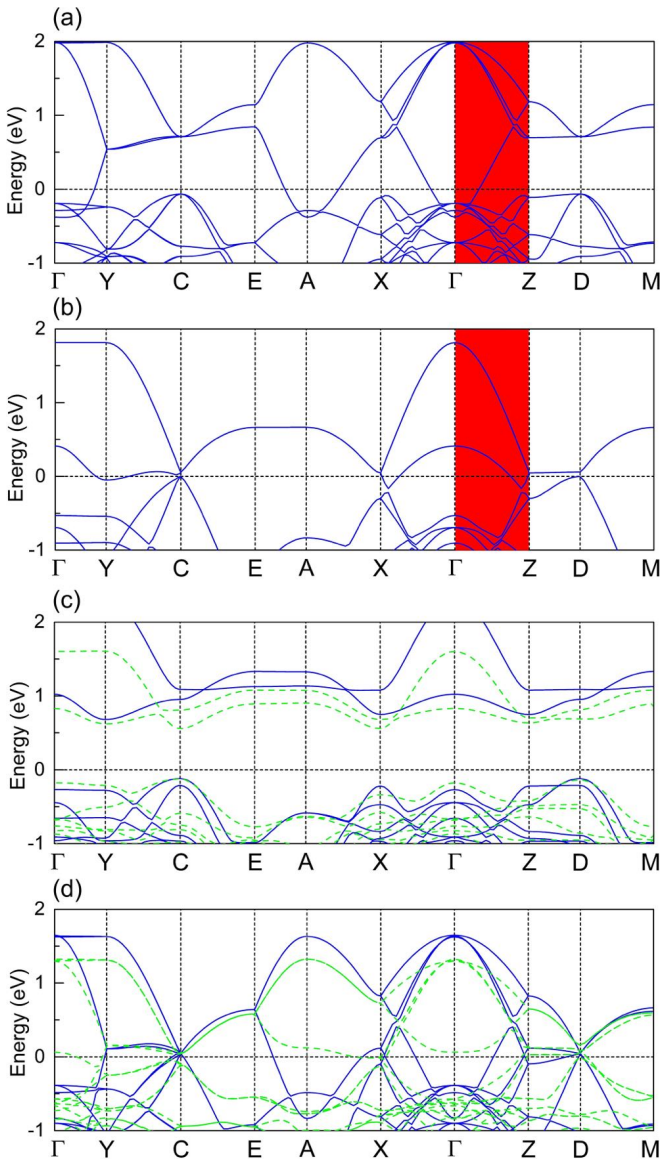
FIG. 7. The band structure of SFO under different conditions. The band structure of (a) cubic SFO with breathing distortion at 2% compressive strain and (b) high-symmetry SFO/YAO superlattice at 2% compressive strain. (c) The comparison of the band structures of SFO/YAO superlattice at 2% compressive strain with breathing distortion (blue curve) and with breathing distortion and rotation and tilt motions (green curve). (d) The comparison of the band structures of cubic SFO (blue curve) and cubic SFO with the fixing of rotation and tilt (green curve).

both B_{oc} and cation ordering partly open the band gap, and the band gap is only opened by combining two factors.

So far, we have explicitly shown that cation ordering instead of rotations plays an essential role in the stability of OO and CO GSs, while previous works on OO LaMnO$_3$ [21] and CO RNO [24] and CFO [23] stress that couplings with rotations are responsible for the appearance of JTD and B_{oc} in the bulk phase. To unearth and distinguish the effect of rotations in bulk materials and superlattices, we now examine the evolution of bandwidth, which strongly determines electron instability in the presence of cation ordering and rotations.
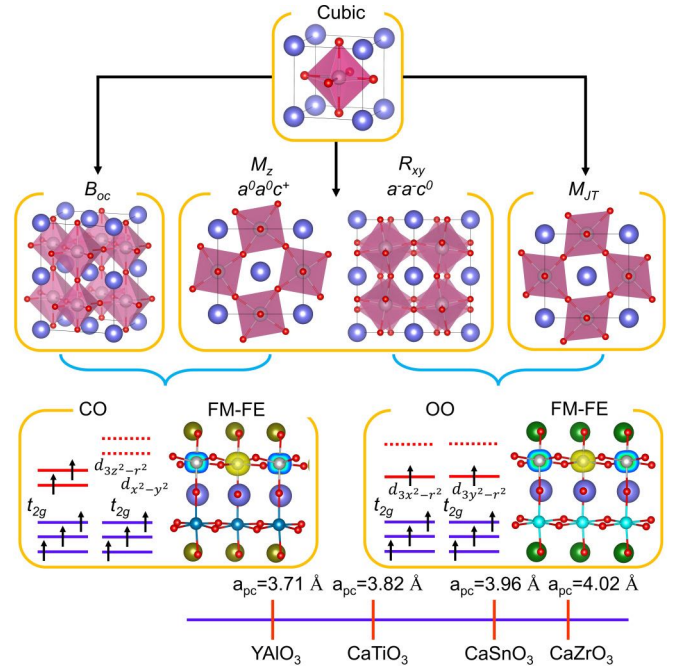

FIG. 8. Design concept for CO and OO multiferroics through superlattice strategy and strain engineering. The possible ABO$_3$ candidates to design SFO/ABO$_3$ CO and OO multiferroic superlattices with their pseudocubic lattice constants are shown at the bottom of the figure.

The calculated band structures of bulk SFO with and without rotations are plotted in Fig. 7(d); the bandwidth of SFO is notably reduced with the condensation of rotations, which is consistent with previous findings in CO RNO [24] and CFO [23]. Upon replacement of one layer of SFO by YAO, we notice that the reduction of bandwidth is even larger than when fixing rotations [see Fig. 7(c)]. Further condensing the rotations only slightly modifies the band structure. The results indicate that the weak coupling between rotations and B_{oc} originates from the fact that the change of bandwidth becomes less effective in the superlattices, as cation ordering already reduces the bandwidth.

D. Orbital ordering or charge ordering ferromagnetic multiferroics

Having shown that cation ordering and strain can successfully realize insulating OO and CO states, we finally focus on the ferroelectricity of SFO/CTO and SFO/YAO (under 2% compressive strain) superlattices and elucidate the design rules to achieve FE FM multiferroics. Due to the hybrid improper mechanism [32,33], the polar distortion is triggered in two superlattices by the trilinear coupling with oxygen rotations. The in-plane polarizations obtained by the Berry-phase methods [40] are 3.2 and 4.4 μC/cm^2 for SFO/CTO and SFO/YAO superlattices. Figure 8 summarizes the general design rule of multiferroics based on cubic and metallic SFO by building SFO/ABO$_3$ superlattices. Rotation and tilt are indispensable to trigger the polar distortion, which can be propagated from the ABO$_3$ layer by selecting $Pnma$ ($a^-a^-c^+$) perovskites. The ABO$_3$ layer, which is insulating and provides negative tetragonal strain, helps stabilize the

OO phase by the confinement effect and strain-JTD coupling, and opens the band gap of the SFO layer by combining cation ordering and JTD. Several candidates like CTO [47], CaZrO$_3$, [48] and CaSnO$_3$ [49] are suitable to design OO multiferroics. The ABO$_3$ layer, which avoids tensile mismatch strain or negative tetragonal strain, makes CO and insulating SFO the GS. In this case, the confinement effect plays a dominant role and opens the band gap together with B_{oc}. SFO/YAO superlattices grown on YAO substrate [50], which provides moderate epitaxial compressive strain, are promising candidates for CO multiferroics.

It is known that the values of Hubbard U and exchange parameter J might affect significantly the properties of strongly correlated systems; it has been demonstrated that larger U and J values are required to accurately describe the structural, electronic, and magnetic properties of strongly correlated perovskites such as LaMnO$_3$ [51] and CaFeO$_3$ [23]. Here, the same U and J values are employed as in previous work on CaFeO$_3$, while it is worth noting that our predictions are robust with respect to a reasonable range of U and J values, as demonstrated in Figs. S6– S8 in SM [44]. The coexistence and coupling among structural, electronic, and magnetic degrees of freedom in correlated electron systems play key roles in the manipulation of desired properties for technological applications [52–60]. Consequently, the coupled orbital, charge, spin, and polarization by geometric strategy makes nonpolar and metallic SFO a promising candidate for future functional applications in electronic devices.

IV. CONCLUSIONS

In conclusion, we performed a thorough analysis of the effects of epitaxial strain, cation ordering, and rotations on the structural and electronic properties of metallic cubic SrFeO$_3$. The results indicate that cation ordering is crucial for the stabilization of both orbital ordering and charge ordering states. Besides, we point out that the strong coupling between rotations and Jahn-Teller or breathing distortion in bulk SrFeO$_3$ is substantially decreased due to the decreased bandwidth in SrFeO$_3$/ABO$_3$ superlattices. The stabilization of two modes does not depend sensitively on the rotations. Going further, we establish the importance of epitaxial strain in tuning the relative stability of orbital ordering and charge ordering phases. The strong strain–Jahn-Teller coupling and weak strain-breathing coupling provide a natural platform to access either ground state by strain engineering. The emergence of the hybrid improper ferroelectricity makes SrFeO$_3$/ABO$_3$ superlattices potential candidates for ferroelectric ferromagnetic multiferroics. It is worthwhile to emphasize that the strategy presented here is a general concept and is applicable to a wide range of materials like BaFeO$_3$, CaFeO$_3$, and RNiO$_3$ to design OO and CO ferromagnetic multiferroics.

[1] E. H. da Silva Neto, P. Aynajian, A. Frano, R. Comin, E. Schierle, E. Weschke, A. Gyenis, J. Wen, J. Schneeloch, Z. Xu *et al.*, Science **343**, 393 (2014).

[2] J. Labbe and J. Bok, Europhys. Lett. **3**, 1225 (1987).

[3] J. G. Bednorz, K. A. Müller, and M. Takashige, Science **236**, 73 (1987).

[4] K.-i. Chahara, T. Ohno, M. Kasai, and Y. Kozono, Appl. Phys. Lett. **63**, 1990 (1993).

[5] R. von Helmolt, J. Wecker, B. Holzapfel, L. Schultz, and K. Samwer, Phys. Rev. Lett. **71**, 2331 (1993).

[6] V. Kiryukhin, D. Casa, J. Hill, B. Keimer, A. Vigliante, Y. Tomioka, and Y. Tokura, Nature (London) **386**, 813 (1997).

[7] S. Catalano, M. Gibert, J. Fowlie, J. Iniguez, J.-M. Triscone, and J. Kreisel, Rep. Prog. Phys. **81**, 046501 (2018).

[8] S. Middey, J. Chakhalian, P. Mahadevan, J. Freeland, A. J. Millis, and D. Sarma, Annu. Rev. Mater. Res. **46**, 305 (2016).

[9] Y. Murakami, J. Hill, D. Gibbs, M. Blume, I. Koyama, M. Tanaka, H. Kawata, T. Arima, Y. Tokura, K. Hirota *et al.*, Phys. Rev. Lett. **81**, 582 (1998).

[10] J. Alonso, M. Martinez-Lope, M. Casais, and M. Fernandez-Diaz, Inorg. Chem. **39**, 917 (2000).

[11] T. Kimura, S. Ishihara, H. Shintani, T. Arima, K. Takahashi, K. Ishizaka, and Y. Tokura, Phys. Rev. B **68**, 060403 (2003).

[12] M. Sánchez, G. Subías, J. García, and J. Blasco, Phys. Rev. Lett. **90**, 045503 (2003).

[13] J. Torrance, P. Lacorre, A. Nazzal, E. Ansaldo, and C. Niedermayer, Phys. Rev. B **45**, 8209 (1992).

[14] M. L. Medarde, J. Phys.: Condens. Matter **9**, 1679 (1997).

[15] J. Alonso, J. García-Muñoz, M. Fernández-Díaz, M. Aranda, M. Martínez-Lope, and M. Casais, Phys. Rev. Lett. **82**, 3871 (1999).

[16] I. Mazin, D. Khomskii, R. Lengsdorf, J. Alonso, W. Marshall, R. Ibberson, A. Podlesnyak, M. Martínez-Lope, and M. Abd-Elmeguid, Phys. Rev. Lett. **98**, 176406 (2007).

[17] P. Woodward, D. Cox, E. Moshopoulou, A. Sleight, and S. Morimoto, Phys. Rev. B **62**, 844 (2000).

[18] T. Akao, Y. Azuma, M. Usuda, Y. Nishihata, J. Mizuki, N. Hamada, N. Hayashi, T. Terashima, and M. Takano, Phys. Rev. Lett. **91**, 156405 (2003).

[19] M.-H. Whangbo, H.-J. Koo, A. Villesuzanne, and M. Pouchard, Inorg. Chem. **41**, 1920 (2002).

[20] J. MacChesney, R. Sherwood, and J. Potter, J. Chem. Phys. **43**, 1907 (1965).

[21] J. H. Lee, K. T. Delaney, E. Bousquet, N. A. Spaldin, and K. M. Rabe, Phys. Rev. B **88**, 174426 (2013).

[22] X. R. Wang, C. J. Li, W. Lü, T. Paudel, D. Leusink, M. Hoek, N. Poccia, A. Vailionis, T. Venkatesan, J. Coey *et al.*, Science **349**, 716 (2015).

[23] Y. Zhang, M. M. Schmitt, A. Mercy, J. Wang, and P. Ghosez, Phys. Rev. B **98**, 081108 (2018).

[24] A. Mercy, J. Bieder, J. Íñiguez, and P. Ghosez, Nat. Commun. **8**, 1677 (2017).

[25] Z. He and A. J. Millis, Phys. Rev. B **91**, 195138 (2015).

[26] L.-t. Jiang, K.-j. Jin, C. Ma, C. Ge, G.-z. Yang, and X. He, Phys. Rev. B **97**, 195132 (2018).

[27] I. Cherair, E. Bousquet, M. M. Schmitt, N. Iles, and A. Kellou, J. Phys.: Condens. Matter **30**, 255701 (2018).

[28] C. Domínguez, A. B. Georgescu, B. Mundet, Y. Zhang, J. Fowlie, A. Mercy, A. Waelchli, S. Catalano, D. T. Alexander, P. Ghosez *et al.*, Nat. Mater. **19**, 1182 (2020).

[29] Z. Liao, N. Gauquelin, R. J. Green, K. Müller-Caspary, I. Lobato, L. Li, S. Van Aert, J. Verbeeck, M. Huijben, M. N. Grisolia *et al.*, Proc. Natl. Acad. Sci. USA **115**, 9515 (2018).

[30] J. M. Rondinelli and N. A. Spaldin, Phys. Rev. B **82**, 113402 (2010).

[31] J. M. Rondinelli and N. A. Spaldin, Phys. Rev. B **81**, 085109 (2010).

[32] E. Bousquet, M. Dawber, N. Stucki, C. Lichtensteiger, P. Hermet, S. Gariglio, J.-M. Triscone, and P. Ghosez, Nature **452**, 732 (2008).

[33] A. T. Mulder, N. A. Benedek, J. M. Rondinelli, and C. J. Fennie, Adv. Funct. Mater. **23**, 4810 (2013).

[34] R. Ramesh and D. G. Schlom, Nat. Rev. Mater. **4**, 257 (2019).

[35] J. P. Perdew, A. Ruzsinszky, G. I. Csonka, O. A. Vydrov, G. E. Scuseria, L. A. Constantin, X. Zhou, and K. Burke, Phys. Rev. Lett. **100**, 136406 (2008).

[36] G. Kresse and J. Furthmüller, J. Comput. Mater. Sci. **54**, 11169 (1996).

[37] G. Kresse and D. Joubert, Phys. Rev. B **59**, 1758 (1999).

[38] V. I. Anisimov, F. Aryasetiawan, and A. Lichtenstein, J. Phys.: Condens. Matter **9**, 767 (1997).

[39] H. J. Monkhorst and J. D. Pack, Phys. Rev. B **13**, 5188 (1976).

[40] R. King-Smith and D. Vanderbilt, Phys. Rev. B **47**, 1651 (1993).

[41] H. T. Stokes, D. M. Hatch, B. J. Campbell, and D. E. Tanner, J. Appl. Crystallogr. **39**, 607 (2006).

[42] H. T. Stokes, D. M. Hatch, and B. J. Campbell, ISODISTORT, ISOTROPY Software Suite, http://iso.byu.edu.

[43] Z. Li, T. Iitaka, and T. Tohyama, Phys. Rev. B **86**, 094422 (2012).

[44] See Supplemental Material at http://link.aps.org/supplemental/10.1103/PhysRevB.106.235156 for the (i) AIMD results of $SrFeO_3$; (ii) comparison of the potential energy surfaces of Jahn-Teller and breathing distortions between first-principles calculations and the fitting curves; (iii) Hubbard U dependent OO-CO phase transition and electronic structure of $SrFeO_3/ABO_3$ superlattice.

[45] A. Togo, F. Oba, and I. Tanaka, Phys. Rev. B **78**, 134106 (2008).

[46] A. Subedi, Phys. Rev. B **95**, 134113 (2017).

[47] S. Sasaki, C. T. Prewitt, J. D. Bass, and W. Schulze, Acta Crystallogr. Sect. C **43**, 1668 (1987).

[48] P. Stoch, J. Szczerba, J. Lis, D. Madej, and Z. Pędzich, J. Eur. Ceram. Soc. **32**, 665 (2012).

[49] A. Vegas, M. Vallet-Regi, J. González-Calbet, and M. Alario-Franco, Acta Crystallogr. Sect. B **42**, 167 (1986).

[50] R. Diehl and G. Brandt, Mater. Res. Bull. **10**, 85 (1975).

[51] T. A. Mellan, F. Cora, R. Grau-Crespo, and S. Ismail-Beigi, Phys. Rev. B **92**, 085151 (2015).

[52] Y.-H. Chu, L. W. Martin, M. B. Holcomb, M. Gajek, S.-J. Han, Q. He, N. Balke, C.-H. Yang, D. Lee, W. Hu *et al.*, Nat. Mater. **7**, 478 (2008).

[53] S. Picozzi and C. Ederer, J. Phys.: Condens. Matter **21**, 303201 (2009).

[54] P. V. Balachandran and J. M. Rondinelli, Phys. Rev. B **88**, 054101 (2013).

[55] H. J. Zhao, W. Ren, Y. Yang, J. Íñiguez, X. M. Chen, and L. Bellaiche, Nat. Commun. **5**, 4021 (2014).

[56] J. Varignon, N. C. Bristowe, and P. Ghosez, Phys. Rev. Lett. **116**, 057602 (2016).

[57] L. Chen, C. Xu, H. Tian, H. Xiang, J. Íñiguez, Y. Yang, and L. Bellaiche, Phys. Rev. Lett. **122**, 247701 (2019).

[58] Y. Zhang, J. Wang, and P. Ghosez, Phys. Rev. Lett. **125**, 157601 (2020).

[59] P. Ghosez and J. Junquera, Annu. Rev. Condens. Matter Phys. **13**, 325 (2022).

[60] J. Zhang, Y. Zhou, F. Wang, X. Shen, J. Wang, and X. Lu, Phys. Rev. Lett. **129**, 117603 (2022).